A Survey of Thunderstorms that Produce Megaflashes across the Americas

Michael Peterson[1]

[1] ISR-2, Los Alamos National Laboratory, Los Alamos, New Mexico

Corresponding author: Michael Peterson (mpeterson@lanl.gov)

Key Points:

- Megaflashes are produced by Mesoscale Convective Systems (MCSs) that grow large electrified stratiform cloud regions over many hours
- We developed a methodology to track thunderstorm systems, including those that produce megaflashes, and applied it to 4 years of data
- Megaflash timing statistics reflect the life cycle of MCSs – with megaflash onset accompanying peak storm sizes / flash rates

Abstract

We previously observed that long-horizontal lightning flashes exceeding 100 km in length, known as "megaflashes," occur preferentially in certain thunderstorms. In this study, we develop a cluster feature approach for automatically documenting the evolutions of thunderstorm systems from continuous lightning observations provided by the Geostationary Lightning Mapper (GLM) on NOAA's Geostationary Operational Environmental Satellites (GOES). We apply this methodology to GOES-16 GLM observations from 2018 to mid-2022 to improve our understanding of megaflash-producing storms. We find that megaflashes occur in long-lived (median: 14 hours) storms that grow to exceptional sizes (median: 11,984 km^2) while they propagate across long distances (622 km) compared to ordinary storms. The first megaflashes are typically produced within 15 minutes of the storm reaching its peak intensity and extent, describing the transition to mature convection. Most megaflashes occur 13 hours after the initial megaflash activity, and are sufficiently close to convection to suggest initiation in the convective line (where GLM has difficulty detecting faint early light sources from these megaflashes). In-situ generated megaflashes are rare, accounting for 2.7% of the sample using a 50 km convective distance threshold, but also tend to larger than normal megaflashes, possibly due to having direct access to the electrified stratiform cloud through which megaflashes propagate.

Plain Language Summary

Long-horizontal "megaflashes" that exceed 100 km in length are now being routinely detected across the Americas by NOAA's Geostationary Lightning Mappers (GLMs). Initial studies on where / when megaflashes arise have shown that these exceptional flashes preferentially occur in certain storms. In this study, we develop a methodology to automatically identify megaflash-producing thunderstorms and track them over time. We apply it to GOES-16 GLM observations to investigate the types of storms capable of generating lightning at the megaflash scale. We found that megaflashes are produced by storms that grow to large sizes over long periods, and these storms can generate megaflashes over many hours. Most of these megaflashes appear to originate from the convective line, but the small numbers of megaflashes generated deep within the stratiform region tend to be larger. These findings are consistent with our understanding of the life cycle of megaflash-producing Mesoscale Convective Systems (MCSs).

1 Introduction

While most lightning is limited in size to ~10-15 km in horizontal and vertical extent by the dimensions of convective cells (Cecil et al., 2005; Bruning and MacGorman, 2013), the lightning that occurs in electrified anvil or stratiform clouds can be substantially larger. Stratiform clouds in organized Mesoscale Convective Systems (MCSs) are particularly prone to generating long-horizontal lightning "megaflashes" (Lyons et al., 2020) – single flashes whose overall extent exceeds 100 km – because they these clouds extend along nearly the entire length of the convective line (up to 1000+ km long), aggregating charted hydrometeors across vast areas into vertically-thin yet horizontally expansive layers via a combination of advection from the convective core and local in-situ electrification processes (Stolzenburg et al., 1994; Stolzenburg and Marshall, 2008; Rutledge and Peterson, 1994; Schuur and Rutledge, 2000;

Carey et al., 2005; Ely et al., 2008). As electrification guides lightning production, both lightning that originates in the convective core before propagating into the electrified stratiform region and lightning initiated deep within the stratiform region have been observed. For example, Lang et al. (2004) identified 39 cases of stratiform +CG lightning in the stratiform region in a small asymmetrical MCS near the Kansas-Colorado border. Thirty of these stratiform flashes (77%) originated in the convective line before coming to ground in the stratiform region, while the remining 9 flashes (23%) originated within the stratiform region.

Optical lightning sensors in geostationary orbit are revealing lightning flashes that reach spatial and temporal scales beyond the prior ground-based and space-based observations (Vonnegut et al., 1985; Lang et al., 2017; Peterson et al., 2017; Peterson et al., 2021-forte). Pixelated space-based lightning imagers such as NASA's Lightning Imaging Sensor (LIS: Christian et al., 2000; Blakeslee et al., 2020) are capable of measuring flash sizes up to megaflash scales (Peterson et al., 2018), but the Low Earth Orbit (LEO) of LIS and its predecessor Optical Transient Detector (OTD: Christian et al., 2003) limited the amount of time spent viewing each storm. It was unlikely to have the sensor over the right storm at the right time to observe a megaflash – and the largest flash in NASA's LIS science data was just 89 km across (Peterson et al., 2017). Ground-based Lightning Mapping Arrays (LMAs: Rison et al., 1999) resolve lightning structure accurately in three dimensions with continuous coverage over a regional-scale domain. The largest flashes recorded by LMAs reach 321 km in horizontal extent (Lang et al., 2017). However, this is close to the maximum effective range of an LMA in a typical site configuration due to the line-of-sight requirement for detection imposed by the signals being detected. Resolving flashes at this scale also requires the unlikely event of the flash being centered over the array.

Operating a lightning imager like OTD or LIS from geostationary orbit allows flash structure to be mapped continuously over a hemispheric-scale domain. In the first year of its public data, the first of these sensors – NOAA's Geostationary Lightning Mapper (GLM: Rudlosky et al., 2019) – more than doubled the previously-established records for megaflash size and duration (Peterson et al., 2020a). The current record extent flash initiated at the rear of the convective line in an MCS over the Gulf of Mexico and expanded laterally along multiple branches until it reached a final extent of 768 km across – encompassing nearly the entire electrified stratiform cloud behind the convective line (Peterson et al., 2022). While exceptionally rare, flashes at this scale are uniquely-impactful events for the number of Cloud-to-Ground (CG) strokes that they initiate over a substantial horizontal distance (~80% of the flash extent) (Peterson and Stano, 2021), and are important for understanding how the accumulation and neutralization of charge in MCSs varies over their life cycles.

The GOES-16 GLM, in particular, offers a unique perspective on megaflash production in the two primary hotspots for large MCSs: the Great Plains in the United States and the La Plata basin in Argentina / Uruguay / Brazil. We have shown that megaflashes – and especially the largest megaflashes – preferentially occur in these hotspots, and are episodic events (Peterson and Stano, 2021). An MCS that generates a 700-km megaflash is likely to generate smaller megaflashes at increased rates (Peterson 2020a). This leads to certain MCSs producing dozens to even hundreds of megaflashes or more over a matter of hours while other, seemingly similar, MCSs produce none. To advance our understanding of how megaflashes arise, this study creates a large catalog of GOES-16 GLM thunderstorms across the Americas and uses it to document

the attributes of megaflash-producing storms at key points in their histories (including the onset of megaflash activity), and how megaflash production changes as the storm evolves over time.

2 Data and Methods

2.1 The Geostationary Lightning Mapper (GLM) and its Operational Data Product

GLM is an optical lightning detector that continuously records the scene below the satellite in a narrow spectral band (777.4 nm, corresponding to an Oxygen emission line triplet) at ~500 Frames Per Second (FPS), and triggers on transient signals consistent with lightning. The energy in each pixel across the GLM imaging array during a single ~2 ms integration frame is compared against the dynamic background, and triggers an "event" if it exceeds the current local instrument threshold. Events in the same frame that fill a contiguous region of the Charge Coupled Device (CCD) imaging array are clustered into "group" features that approximate distinct lightning pulses, and groups containing events that occur in close spatiotemporal proximity are clustered into "flash" features (Goodman et al., 2010; Mach. 2020).

The hierarchical cluster feature data generated by GLM is then gridded into meteorological imagery products (Bruning et al., 2019). These grids are generated by reprojecting and interpolating GLM event pixel polygons onto a desired output grid, and then aggregating parameters describing the flashes that extend into each pixel on the grid. For example, the Flash Extent Density (FED: Lojou and Cummins, 2004) product describes spatial variations in flash rate. Local maxima in FED imagery correspond to locations of individual convective cells, whose flash rates can be trended over time to infer changes in convective intensity. Meanwhile, Average Flash Area (AFA) and Minimum Flash Area (MFA) describe spatial variations in flash size. These products are useful for differentiating convective regions with small flashes from electrified stratiform or anvil clouds with large flashes.

However, the operational GLM data provided by NOAA, and the gridded products generated from these data, are subject to degradations that limit their ability to describe lightning and thunderstorm trends - and this impacts their utility in scientific research. In order to ensure that GLM meets its latency requirement, the ground system software (Goodman et al., 2010) imposes hard limits on the permitted complexity of groups and flashes. Any group or flash that exceeds these thresholds is terminated, and a new independent feature is generated from any subsequent activity reported by the sensor. Long-horizontal stratiform flashes, in general, and megaflashes, in particular, are artificially split into multiple or even dozens of degraded "flash" features - each capturing a portion of the larger flash.

In addition to being constructed from degraded GLM observations, the standard gridded products are also impacted by radiative transfer effects that cause flash properties and the extent of the thunderstorm to be misrepresented. Nominally, the optical emissions generated by lightning transmit to the top of the cloud where they are detected by GLM. However, light can also take other paths to reach the sensor. For example, photons generated by lightning sources near the edge of convection often escape out the side of the storm and reflect off neighboring cloud faces to reach the satellite (Peterson, 2020b). This generates GLM events in regions that do not produce any lightning while simultaneously causing the flash area to be substantially over-

146 estimated. The largest single groups exceed 10,000 km^2 in area (Peterson et al., 2017),
147 dominating the overall footprint of the flash. The gridded products in regions outside of the
148 primary thunderstorm are populated by only this single group and the properties of its parent
149 flash. As a result, the AFA / MFA grids would report values of 10,000 km^2 - implying the
150 presence of long-horizontal lightning discharges that do not exist.

151 2.2 Producing Science-Level GLM Data

152 Fortunately, the issues with the operational GLM data can be resolved by reprocessing
153 the data. We developed a software package that automatically identifies and repairs GLM flashes
154 in the operational data product, computes additional parameters to better describe the lightning
155 activity recorded by GLM (including new "series" and "area" feature levels describing periods of
156 near-continuous illumination within flashes, and thunderstorm snapshots, respectively), and then
157 generates science-level flash data and gridded products from the repaired observations (Peterson,
158 2019).

159 Our gridded products differ from the standard products distributed by NOAA by focusing
160 on group data that is largely insensitive to radiative transfer effects instead of the event pixel
161 data. We use GLM groups to derive flash skeletons that approximate the lateral structure of the
162 branches in each flash. This is done by connecting each group with its nearest preceding group
163 and rendering the resulting line segment on the desired output grid. Once we have these
164 skeletons, we define the feature boundaries by smoothing the skeletons with a Gaussian kernel
165 and normalizing the results to unity. We define the kernel such that 4 standard deviations occur
166 within the 16.5 km GLM group-to-flash clustering threshold. This value was approximated from
167 analyses of ground network location accuracy statistics from carefully-selected cases near the
168 satellite subpoint where the absence of significant parallax (Virts and Koshak, 2020) causes
169 location uncertainty to be synonymous with location accuracy.

170 We use this approach to compute similar products to the standard GLM meteorological
171 imagery (FED, etc.), replacing event-derived parameters (e.g., AFA, MFA) with group-derived
172 parameters (e.g., Mean Flash Extent, Minimum Flash Extent – both computed from the
173 maximum separation of groups in each flash). We also compute new gridded products based on
174 prior lightning research (Peterson and Rudlosky, 2019; Peterson et al., 2020b). The key grid that
175 we will use in this study is the Convective Probability grid that uses the fractions of long-
176 horizontal flashes (found in stratiform and anvil clouds) at each point to estimate the probability
177 that it represents a convective cloud.

178 2.3 Creating Time-Varying Storm Features from GLM Science Data

179 While our GLM science data contains area features, which were computed for OTD and
180 LIS but omitted in the operational GLM data, these features only represent thunderstorm
181 snapshots, not complete storms. There are multiple approaches that could be taken to link
182 thunderstorm snapshots over time. Because we are interested in megaflash-producing
183 thunderstorms that tend to be large, organized convective systems, we elect to link thunderstorm
184 snapshots based on geospatial overlap between subsequent data packets in our science-level
185 GLM data, which are produced at a 15-minute cadence. This approach will cluster all convective
186 cells within the larger system into a single feature that is tracked over time. It is adequate for

monitoring system-level evolution, but cannot track the behavior of individual convective cells within the broader system.

To identify this overlap, we construct Regions of Interest (ROIs) corresponding to each thunderstorm area using the same approach that we employ to derive our gridded products. The flash skeletons in each area are rendered on a standardized 0.02 degree cylindrical grid, expanded using a Gaussian kernel, and then overlaid on the output grid. ROIs are identified as contiguous regions with lightning activity on the output grid. Note that this contiguous pixel requirement will cause some areas to contain multiple ROIs, making the ROIs essentially lower-level features that are the children of areas in our GLM clustering hierarchy. We then cluster ROIs into time-varying thunderstorm (TS) features if they share a pixel on the standardized output grid within a 60-minute time period. The large time window accommodates intermittent activity in low flash rate storms at the risk of potentially merging separate convective features. But it also natively handles cell merging and splitting, assigning the smaller-scale features to the same broader TS.

There are two key issues that are expected to arise when creating TS features due to the operational nature of the GLM data. The first issue is contamination from instrument artifacts that are present in NOAA's data product. These include both solar artifacts (Peterson, 2020a) and imager artifacts like the "Bahama Bar" (Bateman et al., 2020). We reduce the impact of these artifacts by not considering any TS feature that only occurs in a single 15-minute data packet. However, solar artifacts that overlap with ongoing thunderstorms and particularly-noisy periods for imager artifacts can still produce TS features that pass our filtering. Due to the typical locations and frequencies of these artifacts, we expect them to only slightly impact the TS statistics. The second issue is the requirement of continuous GLM observations to capture complete TS features. While our collection of GLM data is nearly continuous, there are occasional data outages – primarily from the cloud-based data providers that we use to acquire the operational GLM data in near real time. Any outage has the potential to artificially terminate all ongoing TS features. When the data pipeline is restored after the outage, new TS features would be defined from the original ongoing features. We mitigate this problem by flagging TS features that occur within 1 hour of a data outage and exclude these degraded features from our analyses.

An example TS feature is shown in Figures 1 and 2. The chosen TS feature corresponds to the MCS responsible for the largest-extent GLM megaflash. The feature is comprised of a series of snapshots in time, each containing collections of distinct ROIs that are linked together by spatial overlap at some point in the history of the TS. The location and overall orientation of the TS feature during each snapshot is depicted in Figure 1a on top of the Advanced Baseline Imager (ABI) 10.3 μm infrared brightness temperature imagery at the time of the record megaflash and the GLM skeleton image of the megaflash. The central points connected with solid white lines denote the TS feature centroid during each snapshot as it propagates first southward over the Great Plains and then eastward over the Gulf of Mexico to the Atlantic Ocean. The exterior points connected with dotted lines to the corresponding centroid point denote the overall extent / orientation of the TS feature during each snapshot – first east-west

oriented, then turning left to have a northeast-southwest orientation as the storm began moving eastward.

The record megaflash occurred nearly a day into the 4-day history of the TS feature. The remaining panels in Figure 1 zoom in on the GLM snapshot to show Mean Flash Extent (Figure 1b), FED (Figure 1c), and a convective mask derived from our Convective Probability product. Pixels are considered "convective" (mask=1; red) if the probability is 50% or greater and "non-convective" (mask=0; blue) if the probability is less than 50%. For each TS snapshot, we record the position / size of the TS feature at that point, the minima, means, and maxima for all of the gridded products within the snapshot footprint, and a list of megaflashes that occurred during the snapshot. The megaflash list includes the standard properties of each flash (i.e., flash extent, duration, energy, etc.) and also the distances between the first group recorded from the megaflash and the nearest convective pixel on the grid (Figure 1d).

Variations in these TS parameters over time are depicted in Figure 2 for the same storm. The points following the TS centroid location from Figure 1 are colored according to the amount of time since the start of the feature (Figure 2a), the TS footprint area (Figure 2b), the TS ROI count (Figure 2c), and the TS megaflash count (Figure 2d). The white outlines around each point are thin when no megaflashes occur, and thick when megaflashes are detected. In this latter case, the width of the outline corresponds to the maximum megaflash extent. Finally, the background imagery overlays the TS snapshot footprints, which are colored by time (i.e., Figure 1a). The TS feature produced its first megaflash 8.5 hours into the storm after a notable increase in TS convex hull area. Megaflash extents grew over the next 15.25 hours before producing the record 768 km megaflash. Megaflash frequency decreased while the storm was over the Gulf, before increasing again as it moved over Florida where the storm disintegrated into dozens of ROIs. Megaflash activity would pick up once again as the storm moved over the Gulf Stream.

TS feature clustering provides a robust framework for describing these storm-level trends. We applied this clustering to GOES-16 GLM observations between January 2018 and July 2022. Thunderstorm ROIs across 155,468 snapshots were clustered into 2,373,178 valid TS features – 22,353 (0.94%) of which contained megaflashes. These TS features are then summarized into databases describing their overall properties (duration, propagation distance, total megaflash count, etc.) and their snapshot properties at specific points in in the storm: the first snapshot, the maximum FED snapshot, the maximum footprint area snapshot, the first snapshot with megaflashes (if one exists), and the final snapshot. These summary databases are available at Peterson (2023).

3 Results

We will use this TS feature framework to compare the properties of all thunderstorms with those that produce megaflashes, and to contextualize megaflash occurrence in the evolution of the larger thunderstorm. We will first examine overall thunderstorm statistics in Section 3.1. Next, we will analyze megaflash timing, including the time of first megaflash occurrence, in

Section 3.2. Finally, we will use megaflash proximity to convective pixels to comment on convective-initiated versus in-situ stratiform generated megaflashes in Section 3.3.

3.1 Overall thunderstorm feature properties

We will begin evaluating our TS features by confirming that we can find expected correlations between feature parameters that should be related. Figure 3 shows two-dimensional histograms for some of these comparisons. The overall distance traveled by a TS feature is compared against the TS duration in Figure 3a. These parameters should be fairly well-bounded with influences from (1) the velocity distribution of the steering winds and (2) additional apparent motion from morphological changes in the storm that affect the centroid calculations (i.e., the formation / dissipation of individual cells within the system). Most of the TS cases can be contained within the region bounded by the two white quadratic curves drawn on the figure. These curves are fits to the maximum (dashed) and minimum (dotted) values of the primary data feature (i.e., with outlier values removed). However, ~1% of all TS features occur outside of this bounded region in appendages that represent either storms that propagate over exceptional distances given their short durations (above the maximum curve) or storms that last for a very long time despite hardly moving on the GLM imaging array (below the lower curve). These out-of-family cases arise from GLM artifacts: solar intrusion cases for the former, and random pixel noise for the latter.

We use the quadratic fits in Figure 3a as maximum and minimum thresholds to filter the combinations of distances and durations that we consider valid in Figure 3b, which compares TS duration against the maximum footprint area of the feature. Data points that only contain TS cases removed by these filters are plotted with light shading. As with distance traveled, the maximum size of a TS feature should be a strong function of its duration because upscale growth occurs over an extended period of time. While the original data had similar appendages to Figure 3a, the filters do a decent job at suppressing these outliers. However, there are still some problematic cases with particularly large areas despite very short durations. To filter these cases, we apply use same technique as before: we fit a curve to the upper boundary of the primary distribution and use the fit as a filter to remove problematic cases.

All distance / duration and maximum area filters are applied in the final two distributions in Figure 3 that describe megaflash activity within the TS features. These combined filters remove just 1.22% of all TS data and 1.28% of TS features with megaflashes, but these outliers include most of the anomalous megaflash-producing storms (Figure 3c) that occur when apparent solar artifacts arise near ongoing convection. These single large flashes can even appear to rival the GLM megaflash records (Figure 3d). All of our subsequent analyses will also apply these filters to remove problematic TS features.

The frequencies of TS features across the GOES-16 GLM FOV and their mean properties are shown in Figure 4. These distributions are constructed using the TS starting position as the location of the storm. Most of the top TS locations for storm initiation in Figure 4a occur in the inner tropics: the Amazon basin and Andes regions extending to Central America, and Intra-Tropical Convergence Zone (ITCZ) latitudes over the Pacific and Atlantic oceans. Enhanced TS activity can also be noted in the Gulf of Mexico, along the Gulf Stream and throughout the Rocky Mountain region. Despite our filtering, instrument artifacts are also still present in the

data – particularly the Bahama Bar extending east from the Bahamas and the linear collections of pixels west of Chile.

These overall distributions are heavily weighted towards frequent isolated thunderstorms rather than organized convective systems. An hour-long single-cell convective storm over Arizona counts the same as an organized MCS over the Great Plains consisting of hundreds of convective cells that persists for more than a day. These different storm modes lead to notable variations in TS properties across the GLM FOV according to the types of thunderstorms that start at each location. TS features that generate megaflashes (Figure 4b) occur at low rates across much of the Americas, but the greatest frequencies are found in Central America, northern South America, along the Andes, over Cuba, and along the Gulf Coast and Gulf Stream. These locations are very different than our past distributions because we are counting any storms that produce even a single 100-km megaflash, rather than the larger 300+ km cases lasting multiple seconds that we typically focus on. The regions of the Great Plains and La Plata basin where these larger megaflashes are common are also home to particularly long-lasting (Figure 4c) storms that propagate exceptional distances (Figure 4d) while attaining exceptional footprint areas (Figure 4e). Because we are locating these storms based on starting location, the North America peaks in these distributions – and also the average megaflash count distribution in Figure 4f) are located between the Front Range of the Rocky Mountains in central Colorado and the Mississippi River. The locations where these megaflashes occur and the ending positions of these large MCSs would be further east and spread over a larger area. In South America, the peaks in the distributions extend across Argentina from the Andes to the Pacific Ocean and have greater amplitudes than in North America.

Our previous megaflash analyses indicated that these thunderstorms capable of producing megaflashes represent a distinct subset of the MCS population, which already encapsulates a small portion of all thunderstorms (i.e., comparing Figure 4a and b). Figure 5 computes histograms of TS properties for all storms in Figure 4 as well as those that produce megaflashes. Figure 5a shows the megaflash count histogram for all unique TS features. While megaflash-producing storms account for just 0.97% of all TS features and ~40% of megaflash-producing storms only generate a single megaflash, certain storms are able to produce hundreds or even thousands of megaflashes over their lifetimes. The top megaflash-producing storm, also from the Great Plains, generated 3,983 megaflashes over its nearly 9-day duration. The TS maximum megaflash size histogram in Figure 5b shows that most of these megaflash-producing storms only generate small megaflashes, near the 100 km threshold. All of the 321+ km megaflashes in our 4.5-year record come from just 196 distinct storms.

Megaflash-producing storms are almost exclusively found at the tail of the storm duration (Figure 5d), storm centroid propagation distance (Figure 5e), and storm maximum footprint area (Figure 5f) distributions. While more than half of the storms in our TS database last less than one hour, terminate < 23 km away from their starting location, and encompass a < 950 km^2 total area, megaflash-producing storms have median durations of 14 hours, propagation distances of 1,166 km, and footprint areas of 23,275 km^2. The fraction of all storms that produce megaflashes (dashed lines) also increases with storm duration, distance, and area, with nearly all of the top

storms by each metric producing at least one megaflash. The larger and longer-lived the storm system, the greater its likelihood of generating megaflashes.

3.2 Megaflash timing within thunderstorm features

We can use our TS snapshot data from key points in each thunderstorm to summarize thunderstorm evolution in all storms and storms that produce megaflashes. The key points that we consider (in nominal time order) are: the TS start, the time of maximum TS FED, the time of the first megaflash produced by the TS, the time of maximum TS footprint area, and the end of the TS. Figure 6 shows histograms of the timing of three of these key points (maximum FED time in Figure 6a, maximum footprint area time in Figure 6b and megaflash onset time in Figure 6c) relative to the TS starting time. TS ending time offsets would be equivalent to the TS duration statistics in Figure 5c.

As we saw previously, the time scales associated with megaflash-producing storms are an order of magnitude longer than ordinary thunderstorms, causing the megaflash cases to account for a high fraction of the storms at the tail of each distribution. The median times of the three key points in Figure 6 for megaflash-producing TS features are all between 6.25 and 6.5 hours after the TS start. While these medians agree with our nominal time order, all three occur within one 15-minute data packet of each other. This implies that, in a statistical sense, the point at which the storm reaches peak convective intensity is not all that far removed from its initial maturation (resulting in the first megaflashes), or its maximum areal extent (balancing the ongoing widespread convection with the production of long-horizontal stratiform flashes).

However, the TS properties in megaflash-producing storms can vary considerably between these key points. Figure 7 shows histograms for three TS snapshot parameters: the maximum FED (Figure 7a), the TS footprint area (Figure 7b), and the TS convective fraction (Figure 7c). All five key points are considered, including the starting and ending snapshots. TS features tend to start and end with low flash rates, even approaching the minimum value allowed by our 15-minute data packets. TS features start with higher peak flash rates than the ending snapshots. This is consistent with initial lightning activity accompanying a burst of convection, while the final lightning activity continues to linger until the accumulated charge has been exhausted. FED values during the first megaflash snapshots and the peak footprint area snapshots are nearly identical with medians of 2.85 flashes/min and 3.53 flashes/min, respectively.

Despite occurring at around the same time, the FEDs in these snapshot are significantly lower than the peak FED snapshot with a median of 10.35 flashes/min. Similarly, the max. FED snapshot and megaflash onset snapshot have comparable footprint area statistics in Figure 7b, which are considerably lower than the max. footprint area snapshot (median: 14,493 km^2 and 15,253 km^2 versus 23,275 km^2). Finally, the megaflash onset snapshot contains smaller convective area fractions in Figure 7e than the other key points in TS features. A major contribution to this non-convective dominance is the partitioning scheme being based on long-horizontal flashes (of which megaflashes are the top cases) ensuring that snapshots containing megaflashes will not be labeled 100% convective. By contrast, 25% of top FED snapshots, 9.6%

of top footprint area snapshots, 98% of TS start snapshots, and 92% of TS end snapshots are characterized as entirely convective.

The timing statistics in Figure 6 only describe the first megaflash in each TS feature. The times of all megaflashes relative to these key points in the TS features are shown in Figure 8. Megaflash frequency peaks in the megaflash onset snapshot, which accounts for 5% of all megaflashes. Many of the storms responsible for these flashes produce megaflashes at one point in their evolution and then never again. Meanwhile, 50% of megaflashes occur 13 hours after the initial megaflash, and 10% occur 46 hours following megaflash onset. These contributions from later megaflash activity delay the timing statistics relative to key frames from Figure 6 towards the end of the storm in Figure 8b-e. The median megaflash time delays are 20.75 hours from TS start, 1.5 hours from the max. FED snapshot, 0.75 hours from the max. convex hull area snapshot, and -21.5 hours from the final snapshot in the TS feature.

3.3 Megaflash distance from convection

In addition to timing, we can also use our TS feature framework to examine the locations where megaflashes occur within the broader thunderstorm system. In particular, we will focus on the distance between the first emissions detected from each megaflash and the nearest convective pixel identified by our cloud type mask. Flashes that initiated within the convective core before propagating into the stratiform / anvil cloud should have their first group close to a convective pixel, while in-situ flashes that began within the stratiform / anvil cloud should be displaced from convective pixels by large distances. By compiling statistics describing these convective distances, we can gauge how common megaflashes of each type are.

However, this methodology has two major caveats that need to be recognized. First, as noted previously, our convective partitioning is based on flash extent. Thus, megaflashes will heavily weight their local gridpoints towards being designated as non-convective clouds. Second, GLM often misses the initial emissions from megaflashes while they are developing through the convective core. This can be noted by comparing the lightning records established by LMAs (Lang et al., 2017) and GLM. The top LMA flash contains frequent sources describing branches extending throughout the convective portion of the storm before the flash later enters the stratiform region and reaches its maximum extent. The top GLM flashes, meanwhile, seemingly begin in the stratiform region at the rear of the convective core, propagate linearly further into the stratiform region, and then branch outward in multiple directions to reach their maximum extents. This is a common feature in GLM megaflashes, not just the record cases, and seems to be related to the initial optical sources being too faint to be seen through the optically-thick cloud medium in the convective core.

Both caveats cause convective-initiated megaflashes to be detected late and significantly separated from convection. For this reason, instead of partitioning our sample of megaflashes into convective-originating and in-situ generated, we will consider the full convective distance distribution. After plotting and analyzing hundreds of megaflash cases, an approximate threshold of < 25 km (~3 GLM pixels) encompasses nearly all of the convective cases that we found, while in-situ stratiform cases were typically > 50 km (~6 GLM pixels) from convection. These are not

hard thresholds and are largely arbitrary. Moreover, intermediate distances between 25 and 50 km contained many examples of both flash categories.

Convective distance histograms for all of the megaflashes in our TS dataset are shown in Figure 9. As this dataset includes mesoscale systems at all stages of development, reductions in small convective flash rates in large mature systems cause convective distances in Figure 9a to exceed 1,000 km in some cases (maximum: 1,384 km). In these cases, the convective pixels in the snapshot are located at the opposite end of the storm from the megaflash activity, and may correspond to a disconnected ROI in the same storm. This scenario is rare, however, and most megaflashes occur within well 100 km of convection. Figure 9b zooms in on this lower portion of the distribution, and overlays the number of nominal GLM pixels that correspond to each distance (dashed vertical lines). The notch at the low end of the distribution is an artifact of grid creation. When the first GLM group in the megaflash occurs at a convective boundary, it may be assigned a convective cloud type (and a convective distance of ~0 km) if there are sufficient convective flashes to generate enough groups to overcome the high group rate from the megaflash. However, this becomes harder to accomplish with large megaflashes a few hundred kilometers across because they produce thousands of groups. In cases where the convective group rate is overwhelmed by the group rate from long-horizontal flashes, the pixel will be assigned a non-convective cloud type, and the convective distance will be between the size of a GLM pixel and the 16.5 km group clustering threshold that we also use to construct our gridded products.

The cumulative distribution in Figure 9b shows that 29% of megaflashes occur within one nominal GLM pixel from convection. This fraction increase to 67% by distances corresponding to two GLM pixels, and 84% by three GLM pixels. These results indicate that the dominant mode of megaflash production across the Americas is through convective flashes accessing the vast electrified stratiform regions adjacent to MCSs. Megaflashes that occur at exceptional distances from convection – 50+ km – only account for 2.7% of the cases in our dataset.

Megaflash frequencies are mapped by convective distance in Figure 10. The overall megaflash distribution in Figure 10a is heavily weighted towards cases in our < 25 km category and includes significant contributions from storms across North and South America, as well as in the adjacent oceans. When we subset the distribution to only include cases with convective distances > 25 km (Figure 10b), >50 km (Figure 10c) or > 75 km (Figure 10d), we primarily lose megaflash cases in land regions outside of the MCS hotspot regions of the Great Plains in North America and the La Plata basin in South America. The Gulf Coast, in particular, appears to be unique for containing particularly high fractions of in-situ generated megaflashes compared to other megaflash-producing regions in the western hemisphere.

We can also analyze megaflash timing and flash characteristics for each distance category from Figure 10. Figure 11 constructs timing statistics relative to key frames in the TS feature from Figure 8. The resulting histograms are not markedly different between each category and suffer from significant variability due to their relatively low (for GLM) sample sizes. For example, even though the categories displaced from convection peak notably later than the all megaflash category in Figure 10b, the cumulative distributions still overlap. Thus, it is not clear

from these statistics whether in-situ generated megaflashes tend to occur later than convective-initiated flashes.

However, one parameter where we can find a clear trend is megaflash extent. Similar histograms to Figure 11 are shown in Figure 12. Megaflashes that occur displaced from convection have a lower fraction of small megaflashes compared to large megaflashes. As a result, the cumulative distributions are ordered by distance with medians of 116 km for all megaflashes, 118 km for >25 km megaflashes, 120 km for >50 km megaflashes, and 124 km for > 75 km megaflashes. We suspect that this is probably due to in-situ megaflashes having an advantage in accessing undisturbed regions of electrified stratiform cloud. The higher flash rates in stratiform clouds closer to convection would deplete the local stored charge, potentially inhabiting flash propagation deeper into the stratiform region. Note that convective-initiated flashes can still grow to enormous sizes when they are able to spread throughout the entire electrified stratiform cloud area. This is what occurred with our 768 km megaflash (which was first detected 31 km from the nearest convection). If prior megaflash activity had disturbed the electrified stratiform cloud at any point within the flash footprint, it might not have been able to attain its record extent, similar to the other megaflashes produced by the storm.

4 Conclusions

Clustering thunderstorm snapshots into time-varying thunderstorm features provides new insights into megaflash production. Only 0.97% of thunderstorms observed by the GOES-16 GLM produce megaflashes, and these storms represent the tail of the thunderstorm duration, distance traveled, and footprint area distributions. In most cases, megaflash activity begins 3.75-8.75 hours (25^{th} – 75^{th} percentile range) after the storm is first detected, with a median of 6.25 hours. By this point in the storm, maximum thunderstorm FED values (median: 2.85 flashes/min) are typically greater than initial convection (median: 0.13 flashes/min), but significantly lower than the peak FED in the storm (median: 10.35 flashes/min). Thunderstorm footprint areas are, likewise, quite large (median: 15,233 km^2), though not the largest in the storm (median: 23,275 km^2), while convective area fractions are particularly low (median: 69%). Despite these differences, the median time offsets of the maximum FED, maximum footprint area, and megaflash onset thunderstorm snapshots from the beginning of the storm differ by only the duration of one of our 15-minute data packets. This period describes the MCS thunderstorm reaching its peak intensity and extent as it matures and begins to produce long-horizontal stratiform flashes.

While the most common scenario is for a thunderstorm to barely reach the megaflash threshold and produce a single megaflash at this time, the sustained MCSs generating hundreds to even thousands of megaflash weight the megaflash statistics such that only 5% of megaflashes occur in the same thunderstorm snapshot as the first megaflash. 50% of all megaflashes observed by GLM occurred at least 13 hours after the thunderstorm produced its initial megaflash. Most of these megaflashes occurred close to convection and were probably cases of convective flashes that were able to access the electrified stratiform clouds where they could grow to become megaflashes. The caveats here are that GLM is known to have difficulty detecting early activity in convective-initiated megaflashes while the leaders are still developing through the convective core, and our GLM-based cloud type algorithm is likely to assign all pixels within a megaflash a non-convective cloud type due to their exceptional group counts. Both factors would inhibit our

identification of megaflashes that start in convection. Still, megaflashes that begin < 25 km (~3 GLM pixels) from convection and are probably of convective origin account for 85% of all megaflashes, while megaflash frequency decreases monotonically out to greater distances. Flashes that occur sufficiently far from convection where poor GLM detection is unlikely to be a concern only account for a small fraction of all megaflashes, constraining the contribution from in-situ stratiform flashes. Still, these distant flashes from any convective pixels have some unique attributes. They account for higher fractions of all megaflashes in the MCS hotspot regions of the Great Plains in North America and the La Plata basin in South America compared to the rest of the continent – particularly along the Gulf Coast. There is mixed evidence for whether they are notably delayed compared to other megaflashes. They also are more likely to produce large-extent megaflashes (>>100 km) compared to small megaflashes (~100 km), and the median flash extent increases consistently with convective distance threshold.

There is much to be learned about how megaflashes arise in only certain mesoscale thunderstorms and what factors control the maximum extent of megaflashes within a given thunderstorm. These initial results highlight the role of storm size and longevity in facilitating megaflash activity. Future work will evaluate microphysical measurements by ground- and space-based radars and passive microwave instrumentation to comprehensively characterize TS features at the onset of megaflash activity. We will also infer local recharge rates between subsequent stratiform flashes to investigate whether charge depletion from prior flashes limits the maximum megaflash extent in a given storm.

Acknowledgments

Los Alamos National Laboratory is operated by Triad National Security, LLC, under contract number 89233218CNA000001.

Open Research

The processed data used in this study are available at the Harvard Dataverse via DOI: 10.7910/DVN/OSV2HU (Peterson, 2023).

References

Bateman, M., & Mach, D. (2020). Preliminary detection efficiency and false alarm rate assessment of the Geostationary Lightning Mapper on the GOES-16 satellite. *Journal of Applied Remote Sensing*, *14*(3), 032406-032406.

Blakeslee, R. J., Lang, T. J., Koshak, W. J., Buechler, D., Gatlin, P., Mach, D. M., ... & Christian, H. (2020). Three years of the lightning imaging sensor onboard the international space station: Expanded global coverage and enhanced applications. *Journal of Geophysical Research: Atmospheres*, *125*(16), e2020JD032918.

Bruning, E. C., & MacGorman, D. R. (2013). Theory and observations of controls on lightning flash size spectra. *Journal of the Atmospheric Sciences*, *70*(12), 4012-4029.

Bruning, E. C., Tillier, C. E., Edgington, S. F., Rudlosky, S. D., Zajic, J., Gravelle, C., ... & Meyer, T. C. (2019). Meteorological imagery for the geostationary lightning mapper. *Journal of Geophysical Research: Atmospheres*, *124*(24), 14285-14309.

Carey, L. D., Murphy, M. J., McCormick, T. L., & Demetriades, N. W. (2005). Lightning location relative to storm structure in a leading-line, trailing-stratiform mesoscale convective system. *Journal of Geophysical Research: Atmospheres*, *110*(D3).

Cecil, D. J., Goodman, S. J., Boccippio, D. J., Zipser, E. J., & Nesbitt, S. W. (2005). Three years of TRMM precipitation features. Part I: Radar, radiometric, and lightning characteristics. *Monthly Weather Review*, *133*(3), 543-566.

Christian, H. J., R. J. Blakeslee, S. J. Goodman, and D. M. Mach (Eds.), 2000: Algorithm Theoretical Basis Document (ATBD) for the Lightning Imaging Sensor (LIS), NASA/Marshall Space Flight Center, Alabama. (Available as http://eospso.gsfc.nasa.gov/atbd/listables.html, posted 1 Feb. 2000)

Christian, H. J., Blakeslee, R. J., Boccippio, D. J., Boeck, W. L., Buechler, D. E., Driscoll, K. T., ... & Stewart, M. F. (2003). Global frequency and distribution of lightning as observed from space by the Optical Transient Detector. *Journal of Geophysical Research: Atmospheres*, *108*(D1), ACL-4.

Ely, B. L., Orville, R. E., Carey, L. D., & Hodapp, C. L. (2008). Evolution of the total lightning structure in a leading-line, trailing-stratiform mesoscale convective system over Houston, Texas. *Journal of Geophysical Research: Atmospheres*, *113*(D8).

Goodman, S. J., D. Mach, W. J. Koshak, and R. J. Blakeslee, 2010: GLM Lightning Cluster-Filter Algorithm (LCFA) Algorithm Theoretical Basis Document (ATBD). NOAA NESDIS Center for Satellite Applications and Research. (Available as https://www.goes-r.gov/products/ATBDs/baseline/Lightning_v2.0_no_color.pdf, posted 24 Sept. 2010)

Lang, T. J., Rutledge, S. A., & Wiens, K. C. (2004). Origins of positive cloud-to-ground lightning flashes in the stratiform region of a mesoscale convective system. *Geophysical research letters*, *31*(10).

Lang, T. J., Pédeboy, S., Rison, W., Cerveny, R. S., Montanyà, J., Chauzy, S., ... & Krahenbuhl, D. S. (2017). WMO world record lightning extremes: Longest reported flash distance and longest reported flash duration. *Bulletin of the American Meteorological Society*, *98*(6), 1153-1168.

Lojou, J.-Y., K. L. Cummins, 2004: On the representation of two- and three-dimensional total lightning information. In Preprints, Conference on Meteorological Applications of Lightning Data (pp. Paper 2.4, AMS Annual Meeting, San Diego, CA, USA)

Lyons, W. A., Bruning, E. C., Warner, T. A., MacGorman, D. R., Edgington, S., Tillier, C., & Mlynarczyk, J. (2020). Megaflashes: Just how long can a lightning discharge get?. *Bulletin of the American Meteorological Society*, *101*(1), E73-E86.

Mach, D. M. (2020). Geostationary Lightning Mapper clustering algorithm stability. *Journal of Geophysical Research: Atmospheres*, *125*(5), e2019JD031900.

Peterson, M., Rudlosky, S., & Deierling, W. (2017). The evolution and structure of extreme optical lightning flashes. *Journal of Geophysical Research: Atmospheres*, *122*(24), 13-370.

Peterson, M., Rudlosky, S., & Deierling, W. (2018). Mapping the lateral development of lightning flashes from orbit. *Journal of Geophysical Research: Atmospheres*, *123*(17), 9674-9687.

Peterson, M. (2019). Research applications for the Geostationary Lightning Mapper operational lightning flash data product. *Journal of Geophysical Research: Atmospheres*, *124*(17-18), 10205-10231.

Peterson, M. (2020a). Removing solar artifacts from Geostationary Lightning Mapper data to document lightning extremes. *Journal of applied remote sensing*, *14*(3), 032402-032402.

Peterson, M. (2020b). Modeling the transmission of optical lightning signals through complex 3-D cloud scenes. *Journal of Geophysical Research: Atmospheres*, *125*(23), e2020JD033231.

Peterson, M. J., Lang, T. J., Bruning, E. C., Albrecht, R., Blakeslee, R. J., Lyons, W. A., ... & Cerveny, R. S. (2020a). New World Meteorological Organization certified megaflash lightning extremes for flash distance (709 km) and duration (16.73 s) recorded from space. *Geophysical Research Letters*, *47*(16), e2020GL088888.

Peterson, M., Rudlosky, S., & Zhang, D. (2020b). Thunderstorm cloud-type classification from space-based lightning imagers. *Monthly weather review*, *148*(5), 1891-1898.

Peterson, M. (2021). Where are the most extraordinary lightning megaflashes in the Americas?. *Bulletin of the American Meteorological Society*, *102*(3), E660-E671.

Peterson (2023). GLM Thunderstorm Features. *Harvard Dataverse,* DOI: 10.7910/DVN/OSV2HU, Version 1.

Peterson, M., & Rudlosky, S. (2019). The time evolution of optical lightning flashes. *Journal of Geophysical Research: Atmospheres*, *124*(1), 333-349.

Peterson, M., & Stano, G. (2021). The hazards posed by mesoscale lightning megaflashes. *Earth Interactions*, *25*(1), 46-56.

Peterson, M., Light, T. E. L., & Shao, X.-M. (2021). Combined optical and radio-frequency measurements of a lightning megaflash by the FORTE satellite. *Journal of Geophysical Research: Atmospheres,* 126, e2020JD034411. https://doi.org/10.1029/2020JD034411

Peterson, M. J., Lang, T. J., Logan, T., Wee Kiong, C., Gijben, M., Holle, R., ... & Cerveny, R. S. (2022). New WMO certified megaflash lightning extremes for flash distance and duration recorded from space. *Bulletin of the American Meteorological Society*, *103*(4), 257-261.

Rison, W., Thomas, R. J., Krehbiel, P. R., Hamlin, T., & Harlin, J. (1999). A GPS-based three-dimensional lightning mapping system: Initial observations in central New Mexico. *Geophysical research letters*, *26*(23), 3573-3576.

Rudlosky, S. D., Goodman, S. J., Virts, K. S., & Bruning, E. C. (2019). Initial geostationary lightning mapper observations. *Geophysical Research Letters*, *46*(2), 1097-1104.

Rutledge, S. A., & Petersen, W. A. (1994). Vertical radar reflectivity structure and cloud-to-ground lightning in the stratiform region of MCSs: Further evidence for in situ charging in the stratiform region. *Monthly weather review*, *122*(8), 1760-1776.

Schuur, T. J., & Rutledge, S. A. (2000). Electrification of stratiform regions in mesoscale convective systems. Part II: Two-dimensional numerical model simulations of a symmetric MCS. *Journal of the atmospheric sciences*, *57*(13), 1983-2006.

Stolzenburg, M., Marshall, T. C., Rust, W. D., & Smull, B. F. (1994). Horizontal distribution of electrical and meteorological conditions across the stratiform region of a mesoscale convective system. *Monthly Weather Review*, *122*(8), 1777-1797.

Stolzenburg, M., & Marshall, T. C. (2008). Charge structure and dynamics in thunderstorms. *Space Science Reviews*, *137*, 355-372.

Virts, K. S., & Koshak, W. J. (2020). Mitigation of geostationary lightning mapper geolocation errors. *Journal of Atmospheric and Oceanic Technology*, *37*(9), 1725-1736.

Vonnegut, B., Vaughan Jr, O. H., Brook, M., & Krehbiel, P. (1985). Mesoscale observations of lightning from space shuttle. *Bulletin of the American Meteorological Society*, *66*(1), 20-29.

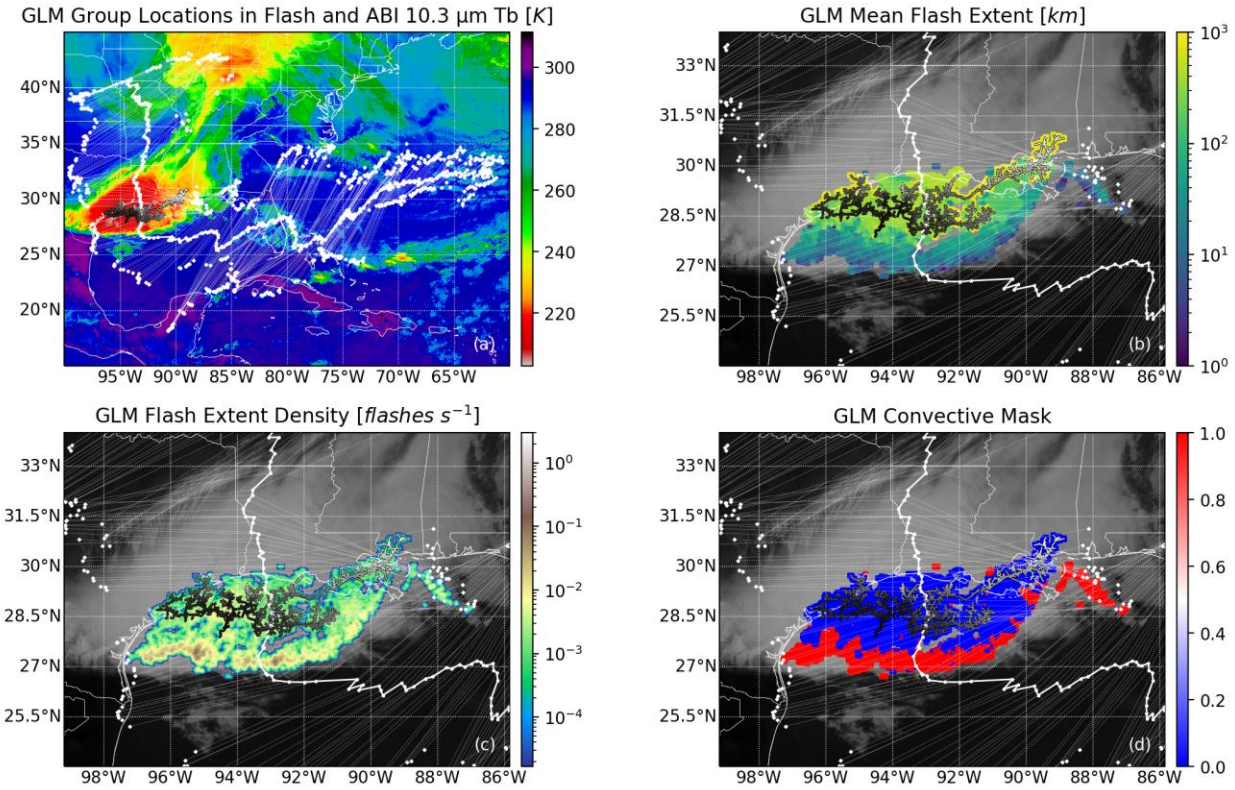

Figure 1. GOES-16 ABI and GLM observations of a snapshot of the TS feature responsible for the current record 768 km megaflash. (a) TS centroids (center white dots connected with white solid line segments) and extremes (white dots connected with dotted lines to the centroid) of each TS snapshot and the record megaflash skeleton are overlaid on ABI 10.3 µm brightness temperature imagery. (b-d) Zoomed imagery adding GLM (b) Mean Flash Extent, (c) Flash Extent Density, and (d) convective cloud mask overlays from the snapshot.

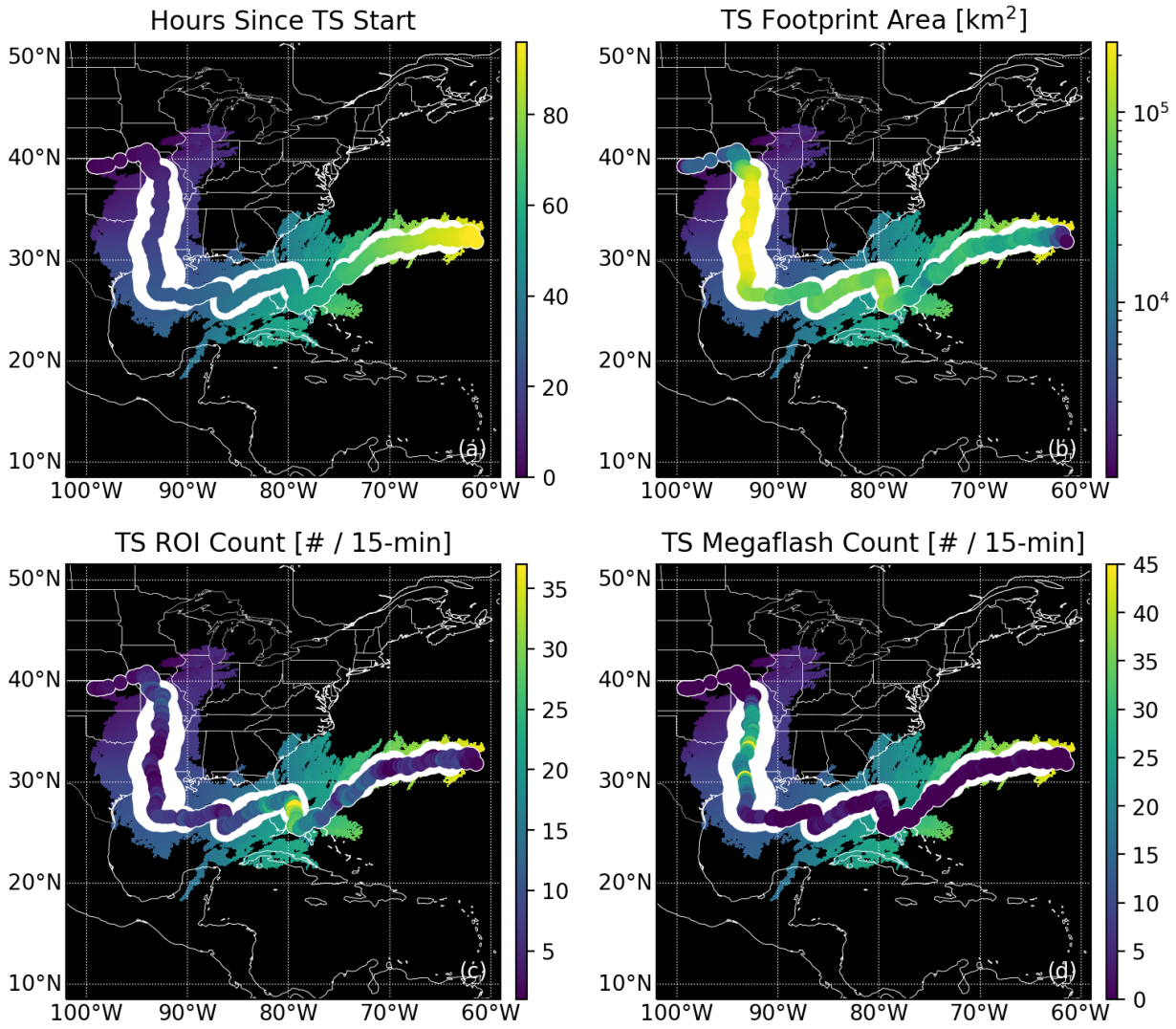

Figure 2. TS feature characteristics during each 15-minute snapshot. Feature (a) duration, (b) footprint area, (c) ROI count, and (d) megaflash count are shown as sequential colored dots overlaid on time-ordered aggregated feature snapshots colored by time. The white border of the centroid dots indicates the absence (thin) or presence (thick) of megaflashes. If megaflashes exist, the thickness of the border indicates maximum flash size during each snapshot.

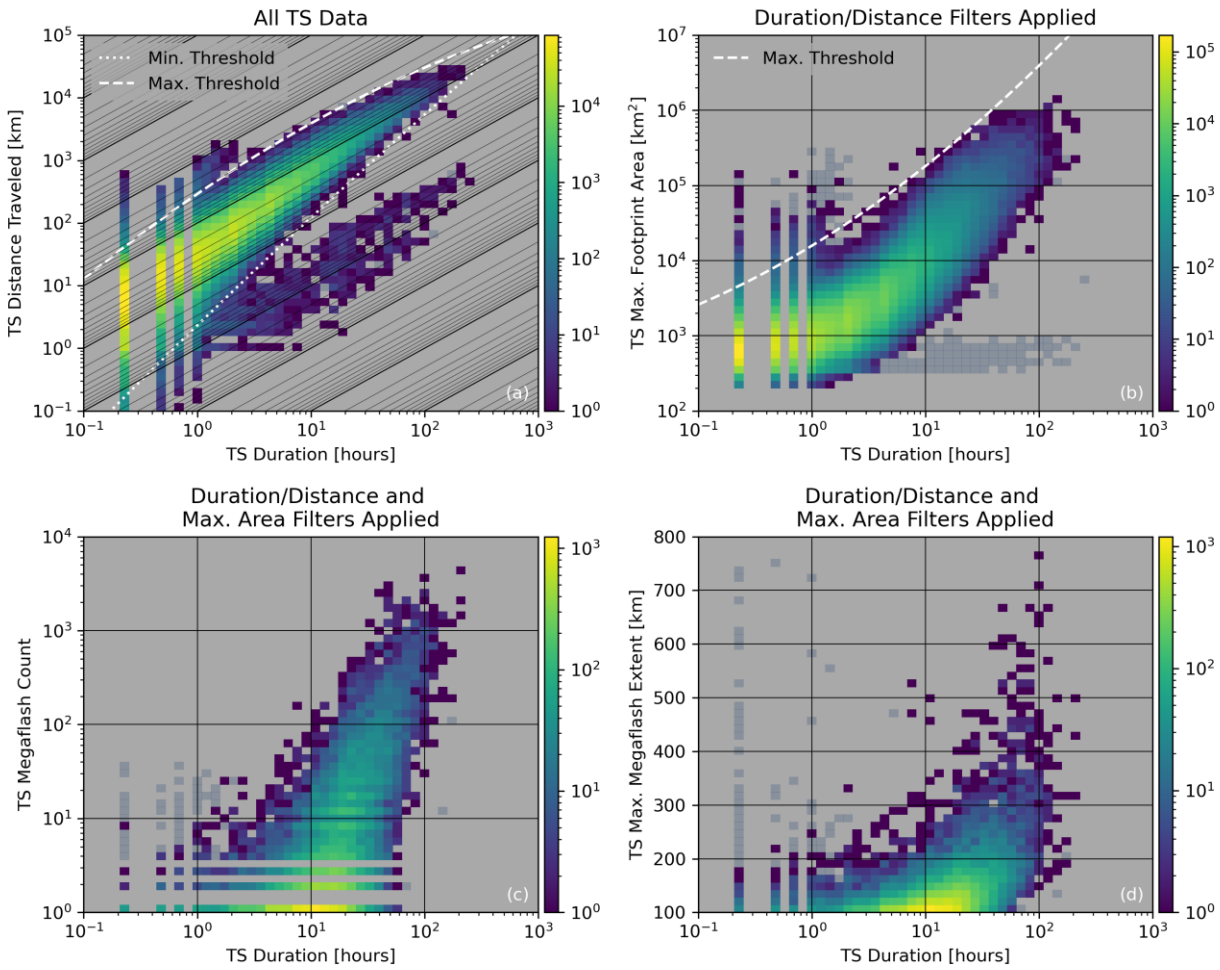

Figure 3. Two-dimensional histograms of TS duration and (a) TS distance traveled, (b) TS maximum footprint area, (c) TS megaflash count, and (d) TS maximum megaflash extent. Dotted and dashed white lines indicate filters that are applied to each subsequent panel. Portions of the distribution removed by these filters are indicated with lighter shading in b-d.

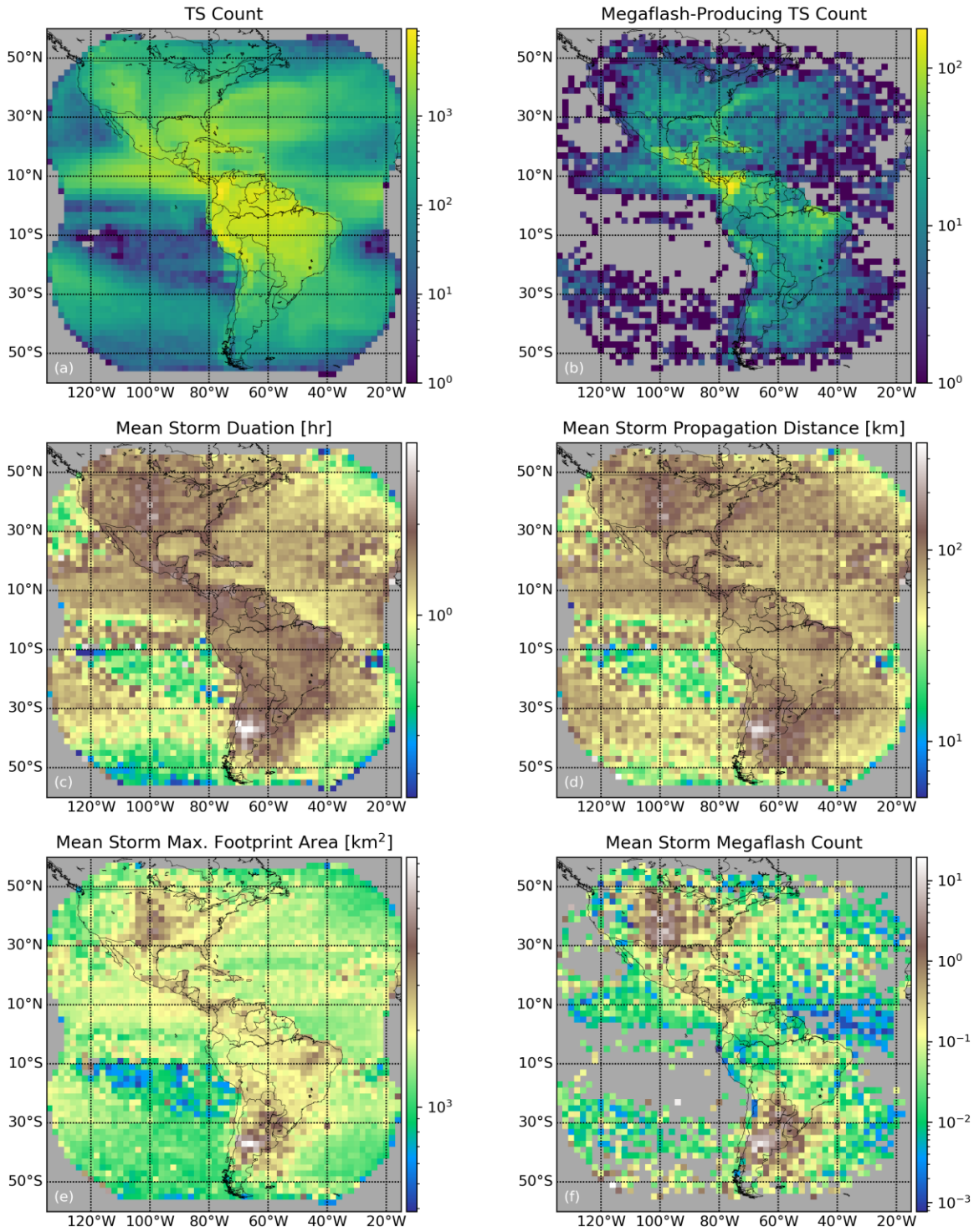

Figure 4. Distributions of (a) all TS features and (b) megaflash-producing TS features across the GOES-16 GLM FOV, as well as average feature (c) duration, (d) propagation distance, (e) maximum footprint area, and (f) megaflash count.

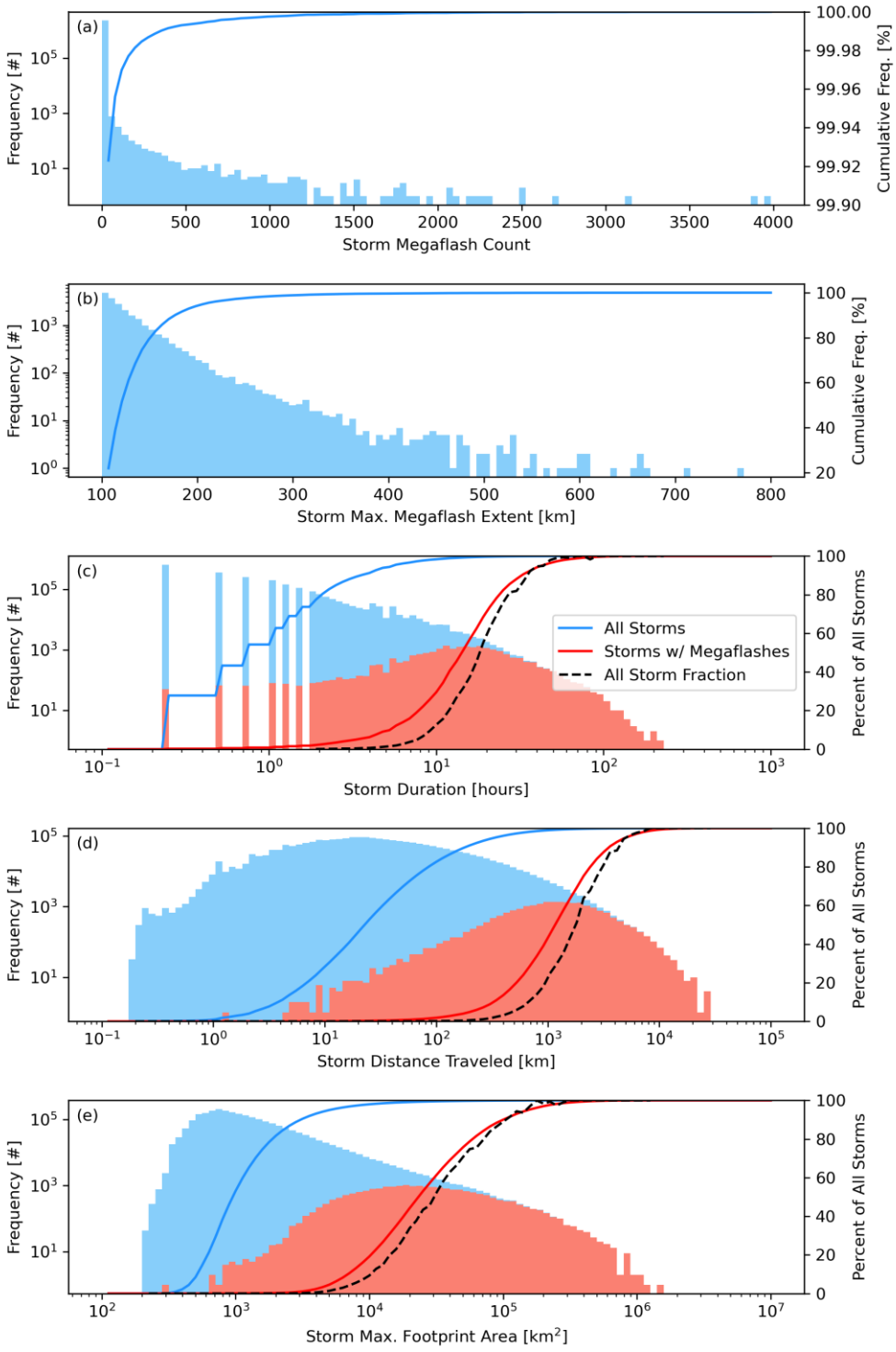

Figure 5. Histograms and cumulative distributions of TS (a) megaflash count, (b) maximum megaflash extent (if present), (c) duration, (d) distance traveled, and (e) maximum footprint area. Separate distributions are shown for all storms and storms with megaflashes. Fractions of all storms in a given bin that produce megaflashes are also indicated on the right axis (black dashed curves).

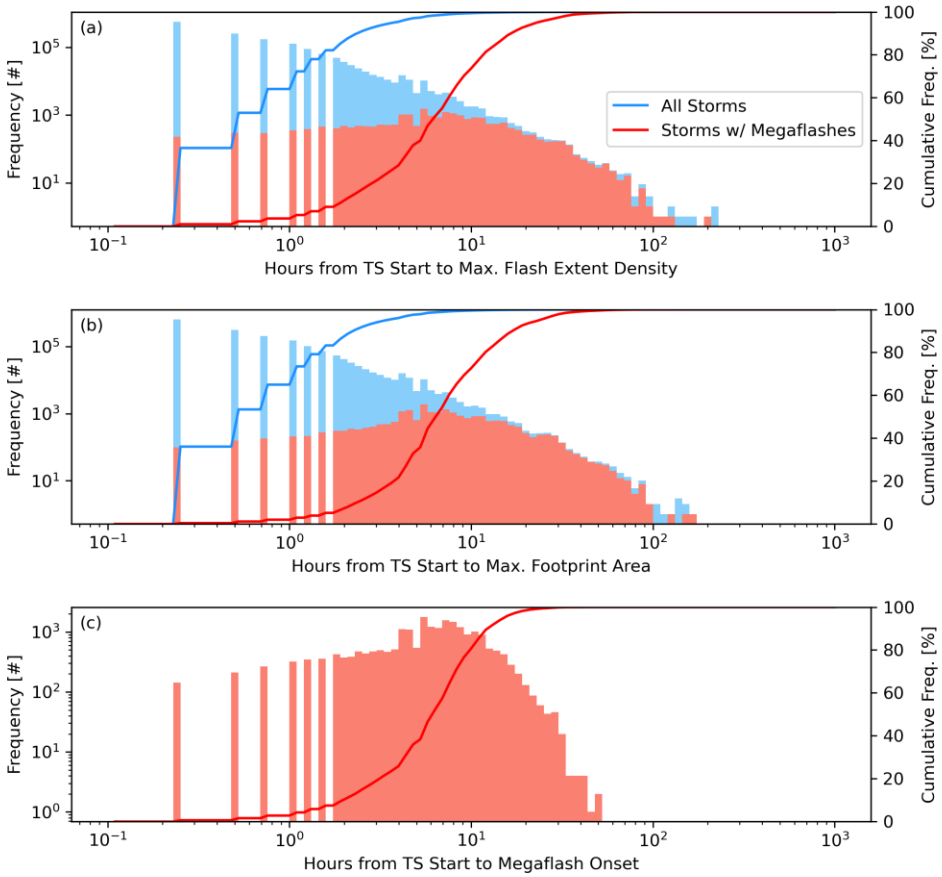

Figure 6. Histograms and cumulative distributions of the time offsets of (a) the maximum Flash Extent Density snapshot, (b) the maximum footprint area snapshot, and (c) the megaflash onset snapshot from the start of the storm. Separate distributions are shown for all TS features and megaflash-producing storms.

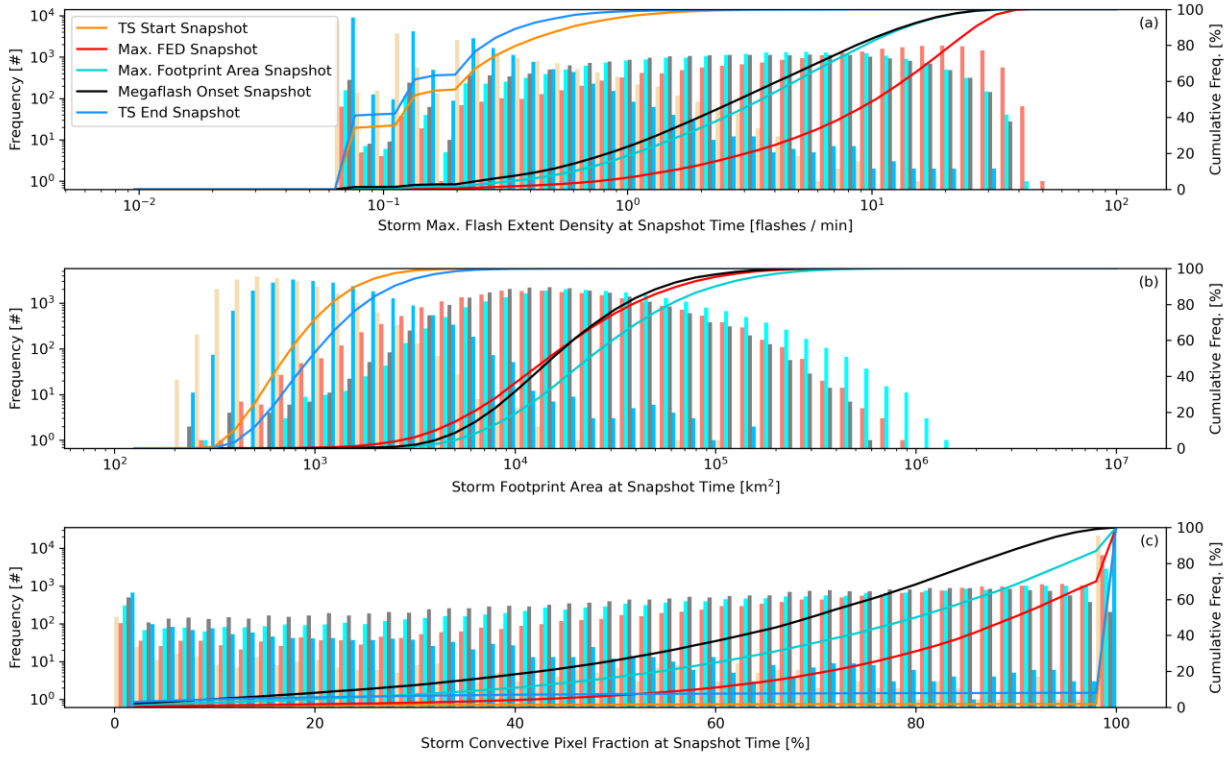

Figure 7. Histogram and cumulative distributions of (a) TS maximum Flash Extent Density, (b) TS footprint area, and (c) TS convective pixel fraction for key points in the storm: the start of the TS, the maximum FED snapshot, the maximum footprint area snapshot, the megaflash onset snapshot, and the final TS snapshot.

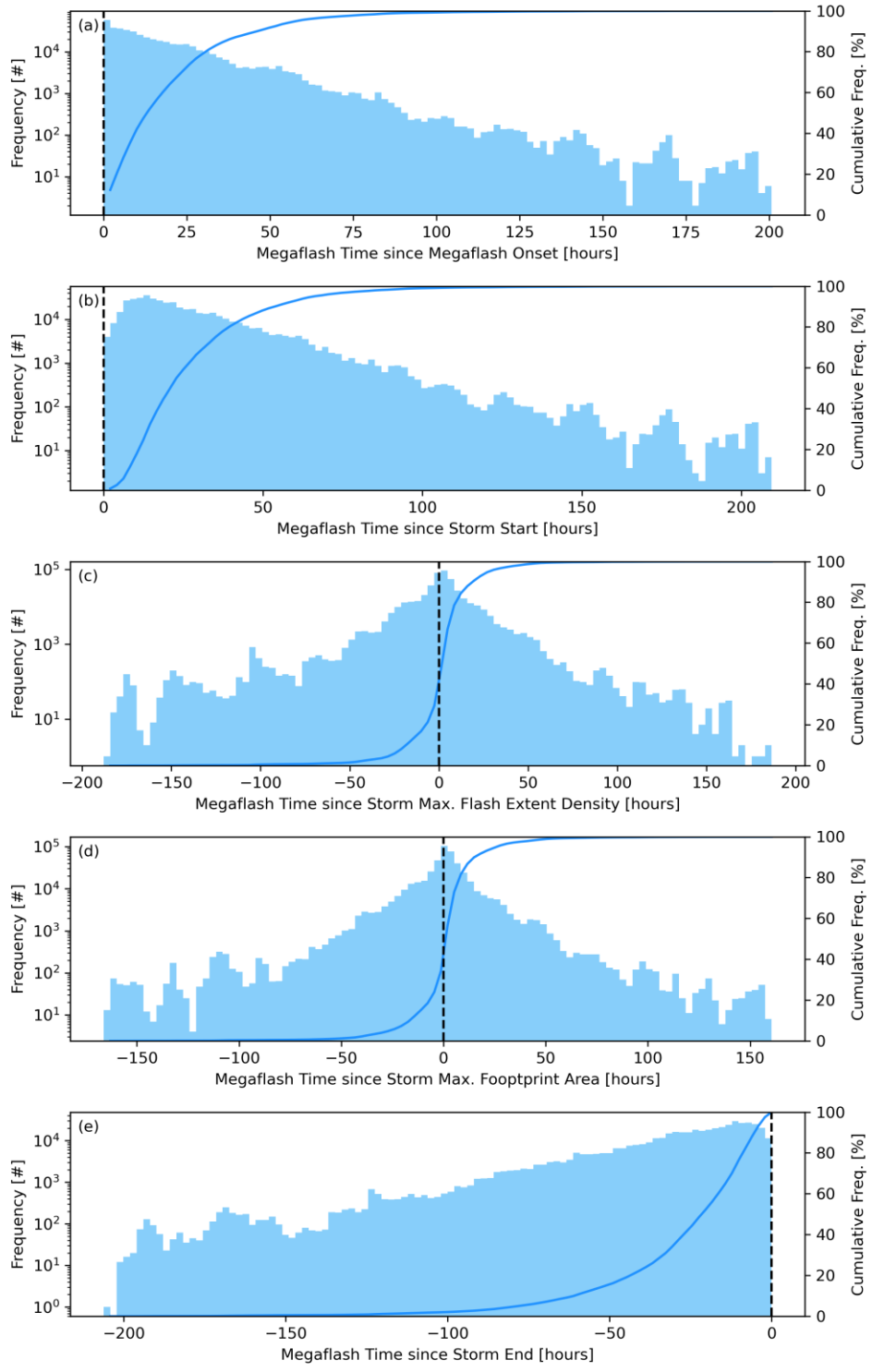

Figure 8. Histograms and cumulative distributions of the time offsets of megaflashes relative to (a) megaflash onset, (b) the TS start, (c) the TS maximum FED snapshot, (d) the TS maximum footprint area snapshot, and (e) the final TS snapshot.

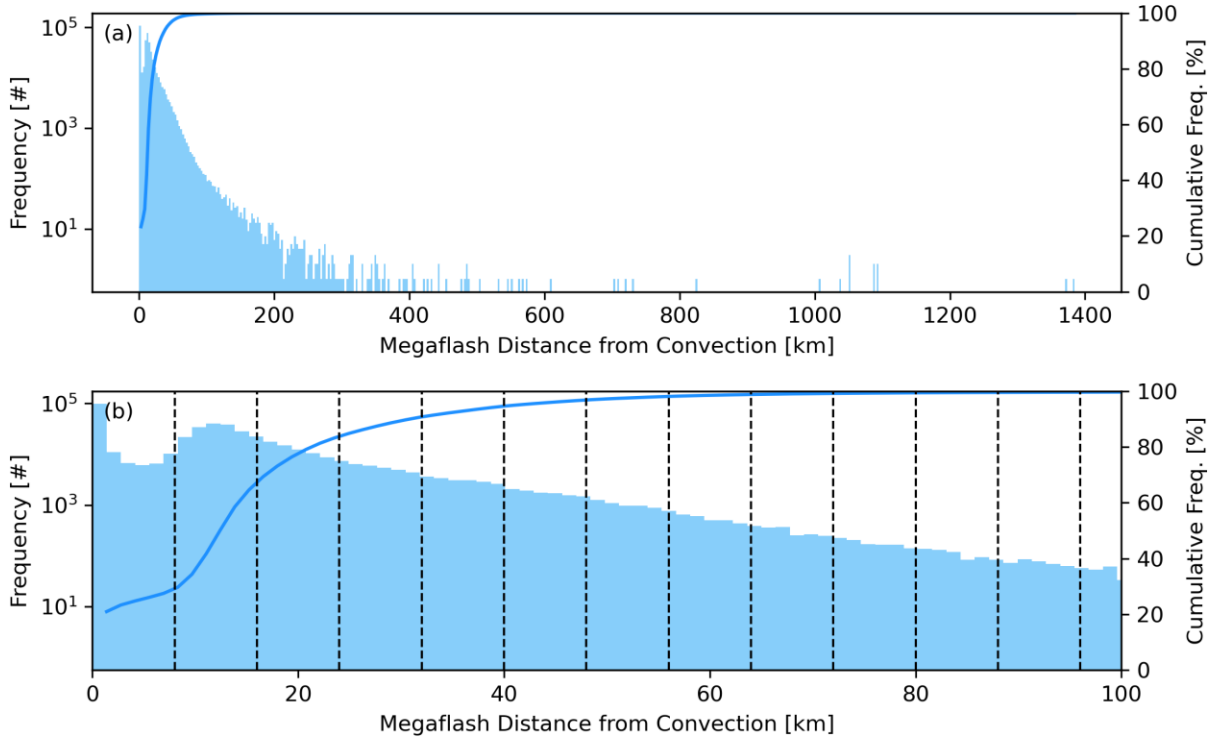

703

704 **Figure 9**. Histograms and cumulative distributions of the distance between the first optical
705 activity detected from each megaflash and the nearest convective pixel. Nominal GLM pixel
706 sizes are overlaid as dashed black lines in the zoomed distribution in (b).
707

708

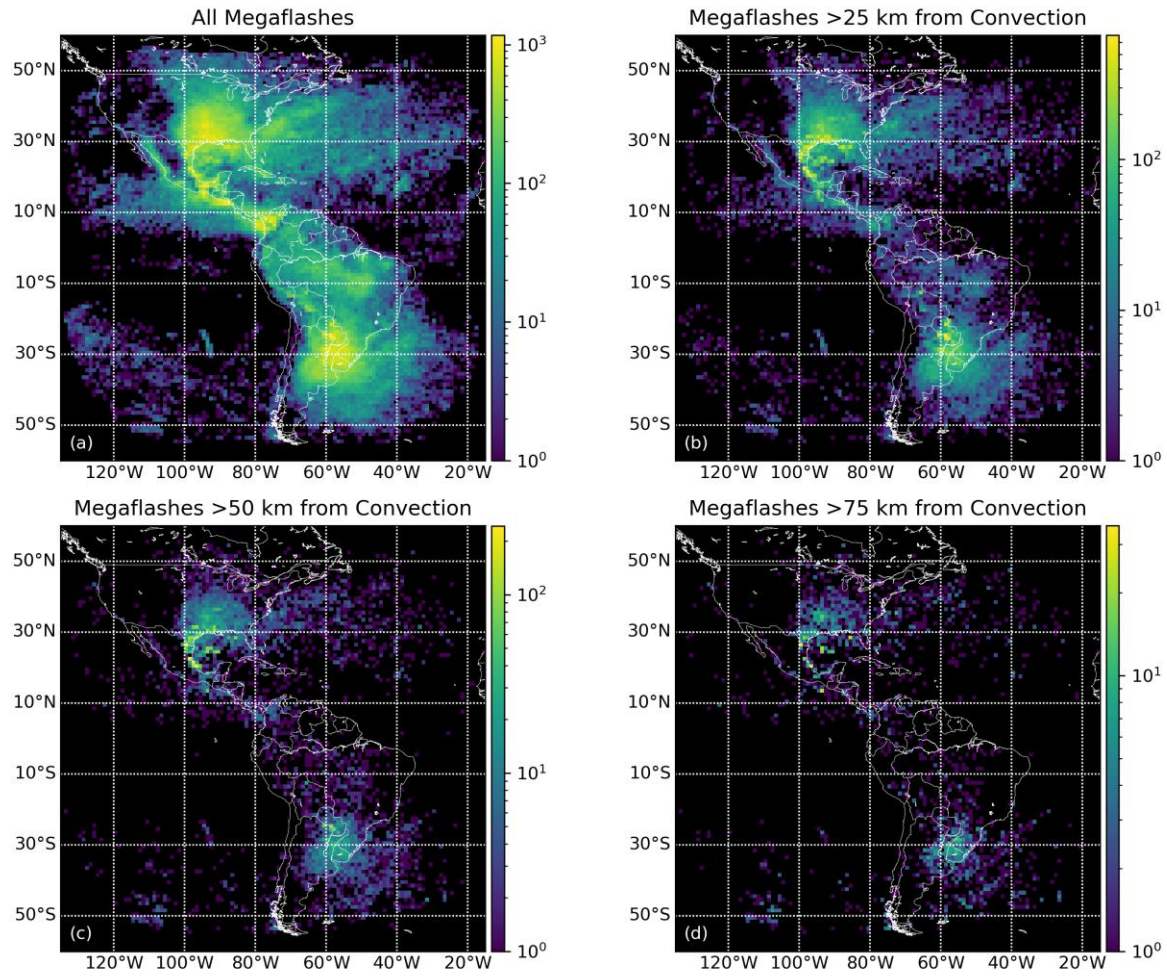

Figure 10. Distributions of (a) all megaflashes and megaflashes (b) > 25 km, (c) >50 km, and (d) >75 km from convection across the GOES-16 GLM FOV.

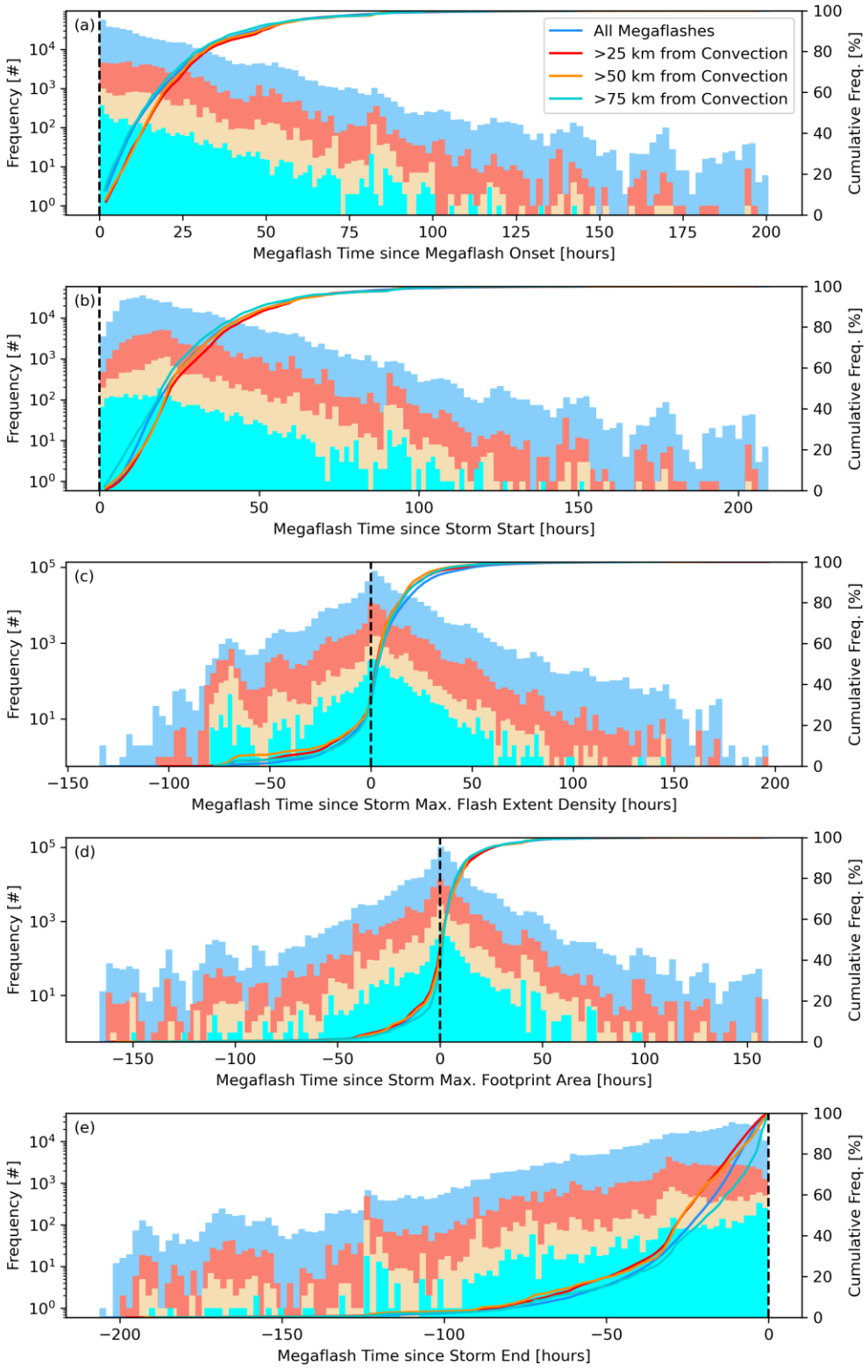

Figure 11. Timing offset statistics, as in Figure 8, but categorized by megaflash distance from convection.

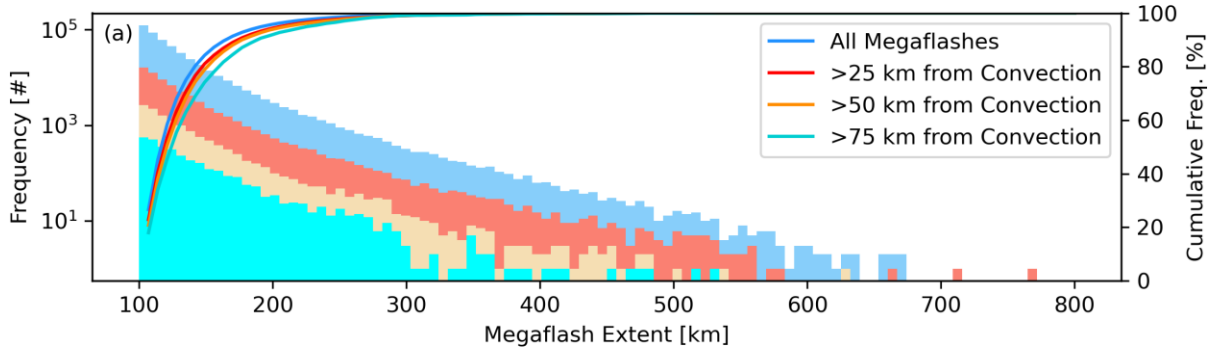

718

719 **Figure 12**. Histogram and cumulative distributions of megaflash extent, categorized by distance
720 from convection.
721